Haverford College

Haverford Scholarship

Faculty Publications   Astronomy

2008

Radio source contributions to the microwave sky

Stephen P. Boughn
Haverford College, sboughn@haverford.edu

Bruce Partridge
Haverford College, bpartrid@haverford.edu

Follow this and additional works at: https://scholarship.haverford.edu/astronomy_facpubs

Repository Citation

"Radio Source Contributions to the Microwave Sky" (with R. B. Partridge), PASP, 120, 281 (2008).

2008

Radio source contributions to the microwave sky

Stephen P. Boughn
Haverford College, sboughn@haverford.edu

R. Bruce Partridge
Haverford College

Follow this and additional works at: http://scholarship.haverford.edu/astronomy_facpubs

Repository Citation

"Radio Source Contributions to the Microwave Sky" (with R. B. Partridge), PASP, 120, 281 (2008).

Radio Source Contributions to the Microwave Sky

S. P. BOUGHN AND R. B. PARTRIDGE

Department of Astronomy, Haverford College, Haverford, PA; sboughn@haverford.edu

ABSTRACT. Cross-correlations of the *Wilkinson Microwave Anisotropy Probe* (*WMAP*) full sky K-, Ka-, Q-, V-, and W-band maps with the 1.4 GHz NVSS source count map and the HEAO I A2 2–10 keV full sky X-ray flux map are used to constrain rms fluctuations due to unresolved microwave sources in the *WMAP* frequency range. In the Q band (40.7 GHz), a lower limit, taking account of only those fluctuations correlated with the 1.4 GHz radio source counts and X-ray flux, corresponds to an rms Rayleigh-Jeans temperature of ∼2 μK for a solid angle of 1 deg^2 assuming that the cross-correlations are dominated by clustering, and ∼1 μK if dominated by Poisson fluctuations. The correlated fluctuations at the other bands are consistent with a $\beta = -2.1 \pm 0.4$ frequency spectrum. *If* microwave sources are distributed similarly in redshift to the radio and X-ray sources and are similarly clustered, then the implied total rms microwave fluctuations correspond to ∼5 μK. While this value should be considered no more than a plausible estimate, it is similar to that implied by the excess, small angular scale fluctuations observed in the Q band by *WMAP* and is consistent with estimates made by extrapolating low-frequency source counts.

1. INTRODUCTION

The only available all-sky survey for radio sources at frequencies above 5 GHz is the *Wilkinson Microwave Anisotropy Probe* (*WMAP*) survey (Hinshaw et al. 2007). The *WMAP* team has cataloged several hundred radio sources detected at flux levels > 1 Jy in one or more of its five frequency bands; a refined search by Lopez-Caniego et al. (2007) has increased the number to nearly 400. Virtually all of these sources are already known from lower frequency radio catalogs such as FIRST, GB6, and the PMN survey in the southern hemisphere (see, for example, Trushkin 2003; Hinshaw et al. 2007; Lopez-Caniego et al. 2007). The *WMAP* sources are a mix of flat spectrum sources, such as quasars, and the brightest "classical" radio galaxies that may have steep spectra, but retain adequate flux in one or more of the *WMAP* frequency bands.

Since the *WMAP* sources do appear in lower frequency catalogs with high probability, it follows that correlating lower frequency catalogs with the *WMAP* images can either identify additional sources, as was found by Lopez-Caniego et al. (2007), or can reveal the statistical properties of sources too weak to be individually detected in the *WMAP* images. In particular, a cross-correlation of the *WMAP* images with lower frequency catalogs can provide information on rms fluctuations induced by such sources at each of the *WMAP* frequencies, and thus average spectral indices for these subliminal sources can be deduced. A related, though simpler, technique was used by Hildebrandt et al. (2007) to examine the contribution of unresolved radio sources to their 11–16 GHz (Cosmological Structures on Medium Angular Scales (COSMOSOMAS) results. We discuss the findings of Hildebrandt et al. further in § 5.3.

Because the subliminal *WMAP* sources that dominate the fluctuations lie roughly in the decade 0.1–1 Jy, they are quite likely to appear in lower frequency catalogs, which generally reach much fainter flux densities, or at least will be correlated with these sources because of clustering. This paper treats the correlation of *WMAP* images at 23, 33, 41, 61, and 93 GHz with number counts from the NVSS 1.4 GHz survey (Condon et al. 1998). Since many flat spectrum radio sources are known to be X-ray emitters, we also cross-correlate the *WMAP* images with the HEAO I A2 2–10 keV all-sky X-ray flux survey.

2. DATA SETS

2.1. HEAO and NVSS Maps

The versions of the HEAO and NVSS maps used in the present analysis were used previously in a variety of analyses, including an investigation of the large-scale structure of the X-ray background (Boughn *et al.* 2002); a determination of the large-scale bias of the X-ray background (Boughn & Crittenden 2004a); and measurements of the ISW effect (Boughn & Crittenden 2002, 2004b).

The NRAO VLA Sky Survey (NVSS) is a flux-limited survey (nominally at 2.5 mJy) at a frequency of 1.4 GHz (Condon *et al.* 1998). It is complete for declinations above $-40°$ and contains 1.8×10^6 sources, with a mean source number density of 51.8 per square degree. The source counts were binned in 24,576 $1.3° \times 1.3°$ pixels. This pixel size is significantly larger than the angular resolutions of all the *WMAP* maps (0.22 to 0.88 degrees) so that the finite resolution effects on the correlation functions are small and yet the pixel size is small enough to yield the large number of pixels required for a

281

statistically significant result. The pixelization we use is a quadrilateralized spherical cube projection (White & Stemwedel 1992). Those pixels that were only partially contained in the survey region were omitted. There are systematic number count offsets that occur in several declination bands that coincide with discontinuous changes in the rms noise levels in the survey (Boughn & Crittenden 2002). To correct for this, random sources were added to or subtracted from each pixel to eliminate the band structure. The resulting map shows no declination dependent structure at a level of < 1%. For comparison, the Poisson noise per pixel is 11%. In order to exclude Galactic sources as well as nearby clusters of galaxies, the map was masked with the most aggressive mask (Kp0) used by the *WMAP* team. In addition, regions that contained pixels with source counts greater than 4σ (corresponding to $\geq 43\%$ of the mean number of sources per pixel) above the average count of 87.5 were masked. This procedure cleaned the map of 10 "objects" located more than 10° from the Galactic plane. Among these are the Orion Nebula and the nearby Virgo, Perseus, and Fornax clusters. That the moderately nearby, rich Coma cluster of galaxies was not one of the regions cut out indicates to us that this masking removed only Galactic and very nearby extragalactic sources. As is the case with the HEAO source masking, the effect of this extra cleaning was primarily to reduce the noise and did not significantly change the value of the correlation with the *WMAP* data. There is a small residual dipole in the NVSS map that is much too large to be that due to the Earth's motion with respect to the comoving frame of the radio sources and, therefore, is undoubtedly due to some large-scale systematic. This dipole moment was fit and removed from the map.

The HEAO1 A2 data set (Boldt 1987) we employ here was constructed from the output of two medium energy detectors (MED) with different fields of view ($3° \times 3°$ and $3° \times 1.5°$) and two high energy detectors (HED3) with these same fields of view. These data were collected during the six-month period beginning on day 322 of 1977. Counts from the four detectors were combined, then pixelized with the same projection used for the NVSS source counts. This MED-HED3 combination was chosen to maximize sensitivity in the 2–10 keV band in which the X-ray background is dominated by extragalactic sources, primarily active galactic nuclei (AGNs). The two angular resolution combinations were then simply added in order to minimize the shot noise in the X-ray signal. The combined map has a spectral bandpass (corresponding to quantum efficiency > 50%) of approximately 3–17 keV (Jahoda & Mushotzky 1989), but the counts have been converted to equivalent flux in the more standard 2–10 keV band. Because of the ecliptic longitude scan pattern of the HEAO satellite, sky coverage and therefore photon shot noise are not uniform. However, the variance of the cleaned, corrected map, 2.1×10^{-2} (TOT cts s^{-1})^2, is significantly larger than the variance of photon shot noise, 0.8×10^{-2} (TOT cts s^{-1})^2, where 1 TOT cts s$^{-1} \approx 2.1 \times 10^{-11}$ erg s^{-1} cm^{-2} (Allen et al. 1994). This implies that most of the variance in the X-ray map

is due to "real" structure. For this reason, and to reduce contamination from any systematics that might be correlated with the scan pattern, we chose to weight the pixels equally.

As with the NVSS map, the HEAO map was masked with the *WMAP* Kp0 mask and then more aggressively masked by removing all pixels within 20° of the Galactic plane and within 30° of the Galactic center. In addition, large regions ($6.5° \times 6.5°$) centered on 92 nearby, discrete X-ray sources with 2–10 keV fluxes larger than 3×10^{-11} erg s^{-1} cm^{-2} (Piccinotti et al. 1982) were removed from the maps. Around the 16 brightest of these sources (with fluxes larger than 1×10^{-10} erg s^{-1} cm^{-2}), the masked regions were enlarged to $9° \times 9°$. We also used the ROSAT All-Sky Survey (RASS) Bright Source Catalog (Voges et al. 1996) to identify additional bright 0.5–2 keV sources. While the RASS survey has somewhat less than full sky coverage (92%), it has a relatively low flux limit that corresponds to a 2–10 keV flux of ~2 × 10^{-13} erg s^{-1} cm^{-2} for a photon spectral index of $\alpha = -2$. Every source in the RASS catalog was assigned a 2–10 keV flux from its hard channel (0.5–2.0 keV) flux by assuming a spectral index of $-3 < \alpha < -1$ as deduced from the hardness ratio within this band. There were 34 sources with fluxes exceeding 3×10^{-11} erg s^{-1} cm^{-2} that were not in the Piccinotti source list, and these were also masked. The HEAO I A2 map itself was searched for "sources" that exceeded the nearby background by a specified amount. Thirty additional such sources at a level of ~3×10^{-11} erg s^{-1} cm^{-2} were identified and masked. These final two cuts amount to only 6.5% of the sky and, in any case, do not significantly change the values of the correlations presented in § 3. The primary reason for masking nearby, strong sources is to reduce the noise in the correlations discussed in § 3. The final masked map has 48% sky coverage. Finally, several systematic foreground features were fit and removed from the map: a linear time drift of detector sensitivity, high latitude Galactic emission, the dipole induced by the Earth's motion with respect to the X-ray background, and emission from the plane of the local supercluster. These corrections are discussed in detail in Boughn (1999) and Boughn et al. (2002).

2.2. Microwave Maps

The microwave data consists of the five frequency bands, K (centered at 22.7 GHz), Ka (33.0 GHz), Q (40.7 GHz), V (60.6 GHz), and W (93.4 GHz), of the three year *WMAP* intensity maps (Hinshaw et al. 2007). These maps were also converted from the available Res 9 HEALPix format to the same $1.3° \times 1.3°$ quadrilateralized spherical cube pixelization of the other two maps. In order to exclude the strong microwave emission from the Galactic plane, all maps were masked with the aggressive *WMAP* Kp0 mask. We note that, in addition, this mask removes all extragalactic microwave sources with fluxes greater than 1 Jy. For comparison, we also analyzed the maps without masking these sources, as discussed in § 5.2. All five maps were corrected for the cosmic microwave background emission by

subtracting the *WMAP* ILC CMB map. Without this correction, the cross-correlations would be dominated by the integrated Sachs-Wolfe effect, the consequence of a universe with a cosmological constant (Boughn & Crittenden 2004b), and, in addition, would be subject to a modest increase in noise. The corrected maps still have a significant component of high latitude Galactic emission, especially on large angular scales. Because fluctuations due to extragalactic sources are predominently on small angular scales, the maps were high pass filtered by simultaneously fitting and removing the dipole, quadrupole, and octopole moments. A Galactic secant law and the Hα map compiled by Finkbeiner (2003), a template for Galactic free-free emission, were included in the fits in order to remove additional Galactic emission. The resulting masked maps were then smoothed with a 24° FWHM Gaussian filter ignoring the contributions of masked pixels. These smoothed maps were subtracted from the corrected maps in order to provide additional high pass filtering. For unmasked pixels near large masked regions, the high pass filtering is somewhat reduced; however, only 1% of these pixels have the effective smoothing area reduced to a value below 0.4 times the nominal and no pixels had effective smoothing areas reduced below 0.11. In any case, the effects of this high pass filter on small-scale fluctuations were minimal, as discussed in § 5.2.

3. CORRELATIONS

Because the primary objective of the present analysis is to constrain the fluctuations of the equivalent brightness temperature due to microwave sources, it might seem reasonable to simply compute the rms fluctuations of the various *WMAP* maps. However, even with the masking, filtering, and corrections discussed in § 2, the rms fluctuations are completely dominated by Galactic emission. In order to isolate that component due to distant extragalactic sources, we cross-correlate the microwave maps with our two templates of extragalactic sources, the NVSS radio source count map and the HEAO X-ray flux map, which is dominated by distant AGNs but could contain flat or inverted spectrum sources not contained in the NVSS survey. The redshift distribution of the signals represented by both of these maps are broad with a peak redshift of $z \sim 1$ (Condon 1984; Dunlop & Peacock 1990; Boughn & Crittenden 2004a). A standard measure of the correlation of two data sets is the cross-correlation function (CCF), which in this case is defined by

$$\text{CCF}(\theta) = \frac{1}{N_\theta} \sum_{i,j} (S_i - \bar{S})(T_j - \bar{T}), \qquad (1)$$

where the sum is over all pairs of pixels i, j separated by an angle θ, S_i is the number of NVSS sources (or the X-ray intensity) in the ith pixel, $\bar{S}$ is the mean number of sources (X-ray intensity), T_i is the *WMAP* equivalent thermodynamic temperature of the ith pixel, $\bar{T}$ is the mean temperature, and N_θ is the number of pairs of pixels separated by θ. Any pair containing a masked pixel is simply removed from the sum. In order to inter-

pret the cross-correlations of the two templates with the microwave maps, it is necessary to determine the rms fluctuations in the template maps as well as the cross-correlation of these two maps. The autocorrelation function (ACF) is defined, using the same notation as in equation (1), as

$$\text{ACF}(\theta) = \frac{1}{N_\theta} \sum_{i,j} (S_i - \bar{S})(S_j - \bar{S}). \qquad (2)$$

Figures 1 and 2 depict the ACFs of the NVSS source counts and X-ray flux. We have corrected the ACF(0) point of Figure 1 for Poisson noise by subtracting 87.5, the mean number of sources per pixel. With this correction, the signal at all angles is an indication of the angular clustering of NVSS radio sources (Boughn & Crittenden 2002). The X-ray ACF at zero lag has been corrected for photon shot noise, but not for the Poisson noise in the distribution of sources because the resolution of the map, 3.04°, is significantly larger than a pixel. However, a model of X-ray clustering indicates that the fraction of ACF(0) due to Poission noise is approximately 77%, coincidentally the same as for the NVSS ACF(0). Figure 3 is the NVSS/HEAO CCF. The (highly correlated) errors in these ACFs and the CCF have not been plotted; however, the signal-to-noise ratio values are large; i.e., S/N > 10 for $\theta \leq 3°$ (Boughn *et al.*2002; Boughn & Crittenden 2004a) and have an insignificant effect on the analysis of this paper.

Figure 4 is the CCF of the corrected NVSS map with the *WMAP* Q-band map. It is clear that only the small angular scale fluctuations of the two maps are correlated. Since the noise in the *WMAP* maps is not well characterized at the level of interest in our analysis, ~1 μK, we chose to estimate the noise by com-

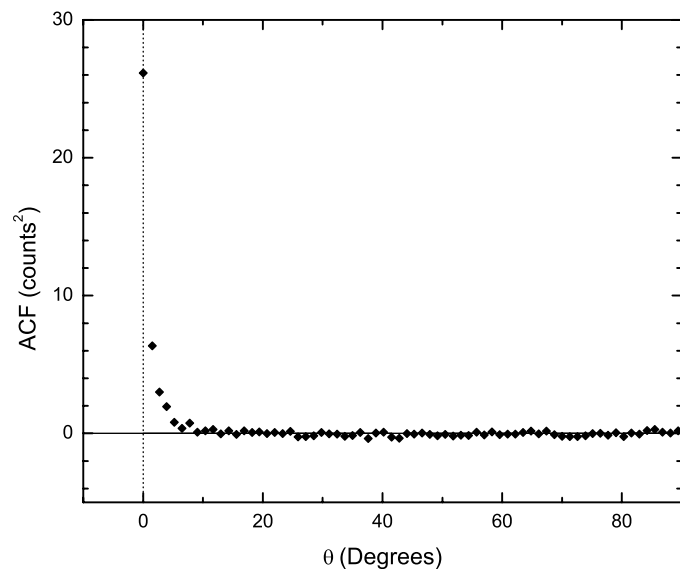FIG. 1.—Autocorrelation function of the NVSS map corrected as discussed in the text. The units are $(\text{counts per pixel})^2$.
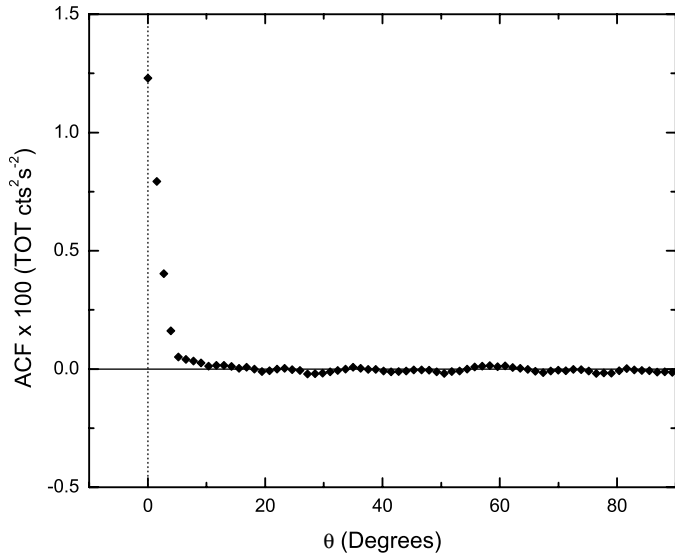
FIG. 2.—Autocorrelation function of the HEAO 1 A2 2–10 keV X-ray map corrected as discussed in the text. $1 \, \mathrm{TOT} \, \mathrm{cts} \, \mathrm{s}^{-1} = 3 \times 10^{-11} \, \mathrm{erg} \, \mathrm{s}^{-1} \, \mathrm{cm}^{-2}$.
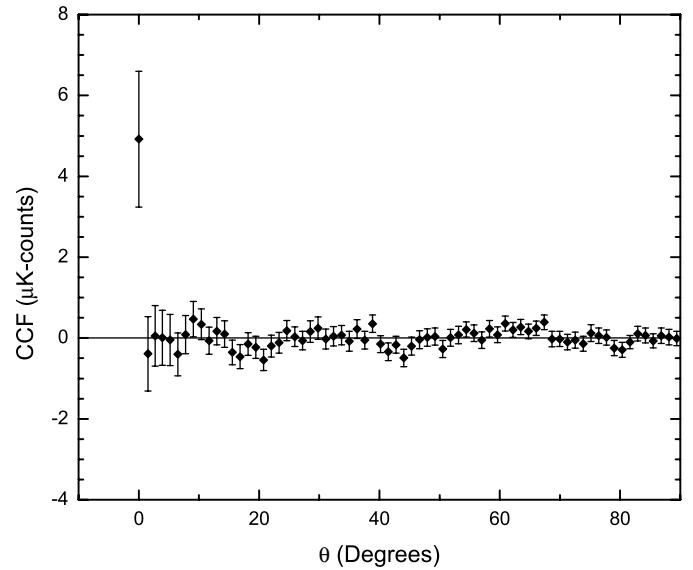

FIG. 4.—Cross-correlation function of *WMAP* Q-band map with the NVSS map. Errors are determined from 240 rotated versions of the data and are highly correlated.

puting 240 CCFs of maps that were rotated with respect to each other. Five rotations were performed about each of 48 uniformly spaced axes separated by ~21°. The resulting distribution of CCFs is, to a reasonable approximation, Gaussian, and so the error bars that are plotted in Figure 4 have the usual 1 σ interpretation. The errors so determined are accurate at the 10% level, which is sufficient for the arguments in § 4. As is clear from the figure, these errors are significantly correlated. This CCF is typical of the CCFs at the other *WMAP* frequencies. Figure 5 shows the dependence of CCF(0) on frequency. The curve represents a power-law microwave spectrum typical of

free-free emission, $T \propto \nu^{-2.1}$, and it is clear that the data are consistent with such a model, although there is no clear detection at the highest (W-band) frequency. The curve is not a fit to the data but is forced to go through the highest signal to noise point at 33 GHz. Formal fits to these data are discussed in § 4. Figures 6 and 7 are the corresponding cross-correlation between Q-band and X-ray maps, and the CCF at zero lag for all *WMAP* frequencies. It is clear that the detection of these correlations is 2 σ at best for the K, Ka, and Q bands, with no significant detection at the V and W bands.

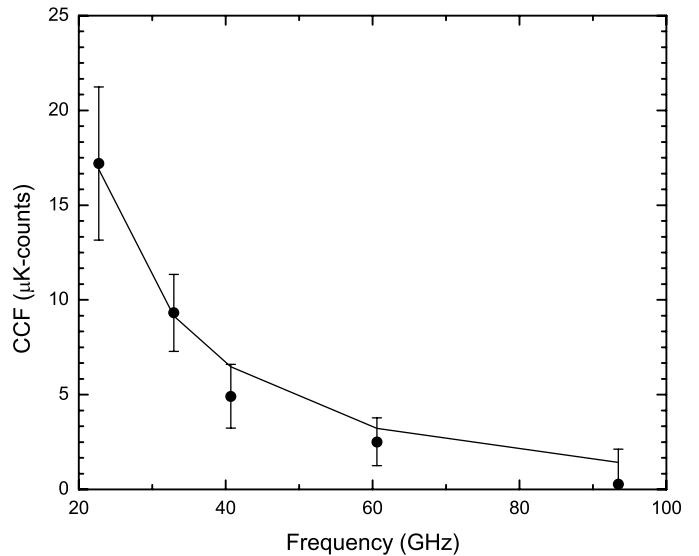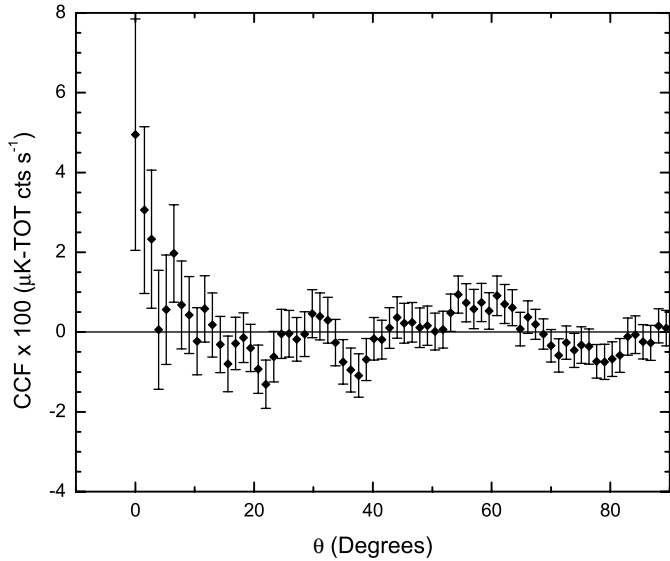FIG. 3.—Cross-correlation function of the X-ray and NVSS maps of Figs. 1 and 2

FIG. 5.—CCF at zero lag of all 5 *WMAP* maps with the NVSS map.

FIG. 6.—Cross-correlation function of *WMAP* Q-band map with the X-ray map. Errors are determined from 240 rotated versions of the data and are highly correlated.

4. CONSTRAINTS ON MICROWAVE FLUCTUATIONS

In order to constrain fluctuations in the microwave sky we assume that the microwave emission M in a given pixel consists of a signal aN proportional to the number N of NVSS sources in the pixels plus a signal C that is statistically independent of N, i.e., $M = aN + C$. Then the zero lag value of the cross-correlation of M with N is given by

$$\text{CCF}(0) = \langle MN \rangle = a\langle N^2 \rangle, \qquad (3)$$
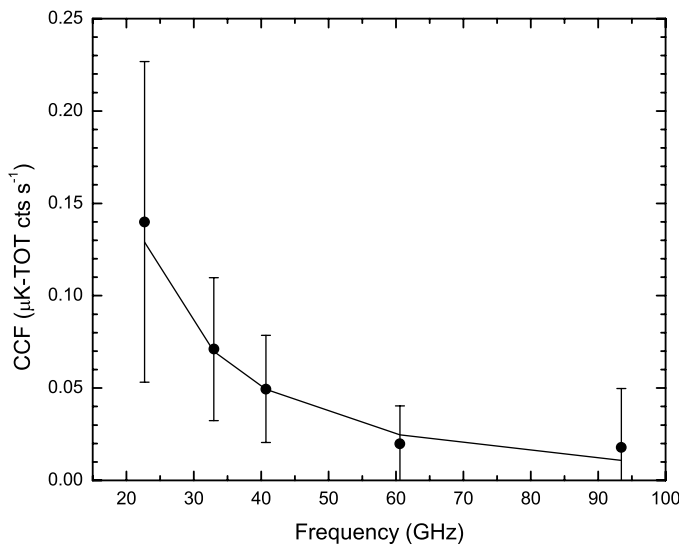
FIG. 7.—CCF at zero lag of all 5 *WMAP* maps with the X-ray map.

where $\langle \rangle$ indicates an ensemble average, in our case to be approximated by the average over the maps. $\langle N^2 \rangle$ is just the NVSS autocorrelation function, which we have measured. Solving for the unknown constant of proportionality gives $a = \langle MN \rangle / \langle N^2 \rangle$. Finally the mean square microwave fluctuation is

$$\langle MM \rangle = a^2 \langle N^2 \rangle + \langle C^2 \rangle + 2a\langle NC \rangle. \qquad (4)$$

Substituting for the constant a and noting that, by assumption, $\langle NC \rangle = 0$, the rms microwave fluctuations are given by

$$\sigma_M = \sqrt{\langle MN \rangle^2 / \langle N^2 \rangle + \langle C^2 \rangle} > \langle MN \rangle / \sqrt{\langle N^2 \rangle}. \qquad (5)$$

Therefore, a lower limit to the microwave fluctuations is given by the *WMAP*/NVSS CCF(0) divided by the square root of the NVSS ACF(0). The error in this lower limit is just the error in the CCF divided by the same factor, $\sqrt{\langle N^2 \rangle}$. Table 1 lists these lower limits for all the *WMAP* frequencies along with those deduced in similar fashion from the *WMAP*/X-ray cross-correlation. No attempt is made to interpret the values of the CCF(θ) for $\theta \neq 0$ since there is no detectable signal in the NVSS CCFs and the finite angular resolution (3.04 degrees FWHM) of the X-ray maps is responsible for most of the signal at $\theta > 0$. It should be noted that the ACF(0) used to deduce the values in Table 1 are those corrected for Poisson fluctuations for both the NVSS and X-ray data. It seems reasonable to do this because it is far more likely that the simple model of proportional emission applies to sources that cluster with each other than the assumption that the Poisson fluctuations of the two populations are correlated. Had we not corrected the ACF(0)s for Poisson fluctuations, then the lower limits in Table 1 would

TABLE 1
<small>LOWER LIMITS ON MICRWAVE FLUCTUATIONS DEDUCED FROM NVSS AND HEAO CROSS-CORRELATIONS.</small>

WMAP Band	Secondary Map	Lower Limits[1]
K Band (22.7 GHz)	NVSS	3.31 ± 0.78
	HEAO	2.57 ± 1.61
	Combined	3.24 ± 1.06
Ka Band (32.95 GHz)	NVSS	1.77 ± 0.39
	HEAO	1.29 ± 0.71
	Combined	1.77 ± 0.41
Q Band (40.70 GHz)	NVSS	0.92 ± 0.31
	HEAO	0.88 ± 0.52
	Combined	$0.85 + 0.45 - 0.26$
V Band (60.60 GHz)	NVSS	0.45 ± 0.22
	HEAO	0.34 ± 0.35
	Combined	$0.40 + 0.44 - 0.15$
W Band (93.44 GHz)	NVSS	0.04 ± 0.29
	HEAO	0.27 ± 0.48
	Combined	$0.24 + 0.63 - 0.22$

[1] Units are μK of rms Rayleigh-Jeans temperature.

the fact that the NVSS and microwave sources are *the same* sources, then it would be appropriate to substitute the total, i.e., not Poisson corrected, ACF(0) (i.e.,$\langle N^2 \rangle$) in equation (5). Because Poisson fluctuations account for 77% of ACF(0) (for both the NVSS and X-ray maps), the lower limits are all reduced by a factor of $\sqrt{1.0/0.23} = 2.1$. The consequences of this will be discussed in the next section. In order to facilitate comparisons with other observations and models we express the above results as the rms temperature fluctuations in a 1 deg^2 top hat beam. This value depends somewhat on the relative contributions of clustering and Poisson noise to the fluctuations. For example, if the Poisson process dominates, then the implied lower limit in 1 deg^2 is $1.9(\nu/40.7 \text{ GHz})^{-2.1}$ μK, while if the fluctuations are dominated by $\sim 1/\theta$ clustering (typical of observations of galaxy clustering—see, e.g., Peebles 1980), then the lower limit becomes $1.4(\nu/40.7 \text{ GHz})^{-2.1}$ μK. If we take as a more reasonable assumption that $\sim 25\%$ of the fluctuations are due to the clustering of sources, comparable to the cases of both NVSS and X-ray fluctuations, then the limit becomes $\sim 1.8(\nu/40.7 \text{ GHz})^{-2.1}$ μK.

5. DISCUSSION

The results presented in § 4 are definitive measurements of the fluctuations in the microwave sky that are correlated either with counts of NVSS radio sources or with HEAO X-ray flux. Even so, they are only lower limits on the total fluctuations in the microwave foreground and the values were deduced under the assumption that correlations were due to joint clustering of microwave, NVSS, and X-ray sources. The power-law fit to the lower limits indicates that the spectral index is more consistent with a flat spectrum such as that characteristic of free-free emission than with the steep spectrum often characteristic of synchrotron emission. This should not be surprising because high frequency observations will naturally be biased toward flatter spectrum sources (e.g., Massardi et al. 2007).

5.1. Estimate of Total Fluctuations

It is possible to make a (slightly) educated guess as to the total level of microwave fluctuations by appealing to the example of NVSS/X-ray correlated fluctuations. The level of X-ray fluctuations correlated with NVSS fluctuations can be deduced in the same manner as in equation (5), i.e., $\langle X^2 \rangle > \langle XN \rangle^2 / \langle N^2 \rangle$. The value of this quantity is 1.6×10^{-3}, whereas the total X-ray fluctuation (see Fig. 2) is $\langle X^2 \rangle = 0.0123$. Hence $\sqrt{\langle X^2 \rangle}$ is a factor of 2.8 larger than the derived lower limit. The same factor applies to the case of a lower limit of NVSS fluctuations derived from X-ray fluctuations because Poisson fluctuations happen to account for the same fraction of total fluctuations in both the NVSS and X-ray cases. As was pointed out in § 2, the NVSS and X-ray fluctuations have similar redshift distributions. *IF* microwave sources also have a similar redshift distribution, *IF* microwave fluctuations have similar ratios

of Poisson to clustering components, and *IF* the uncorrelated component (*C* in eq. [4]) composes the same fraction of the X-ray fluctuations as of the microwave fluctuations, then one would expect the same 2.8 correction factor to apply. This would imply that the total microwave fluctuations would be $\sim 5(\nu/40.7 \text{ GHz})$ μK. While plausible, there is no direct evidence that the three above conditions are true. Therefore, this conclusion should be considered only as a plausibility argument.

It was pointed out above that had total ACF(0)'s, including the Poisson contributions, been used to determine correlated microwave fluctutations, then the derived lower limits would be a factor of 2.1 less than those listed in Table 1. A similar analysis using the NVSS/X-ray correlation to determine a lower limit to the X-ray fluctuations would have resulted in a lower value by this same factor. However, the factor by which the actual X-ray fluctuations exceed the correlated component would have increased by precisely the same factor. Therefore, while the lower limits depend on whether the correlated fluctuations are clustering or Poisson dominated, the rough estimate of *total* fluctuations does not.

5.2. Potential Sources of Systematic Error

All of the analysis described above was for *WMAP* maps that were masked for all regions that contained microwave sources that exceeded 1 Jy. We repeated the analysis not excluding these sources (but retaining the mask of the Galactic plane). The K- and Ka-band lower limits both increase by a factor of 1.4 while the Q-band lower limit increases by a factor of 1.6. Given the limited signal-to-noise ratio, these factor are consistent with each other, and our conclusions about the spectral index of fluctuations in the microwave sky remain unchanged.

There may be some question as to whether the high pass filtering discussed in § 2 reduces the CCF(0) and hence the lower limits derived in this paper. As an estimate of the significance of this effect, the same procedure described in § 2 was performed on the NVSS map, which was then cross-correlated with the unfiltered NVSS map. The result was a negligible (1.5%) decrease from the ACF(0) value of the original NVSS map. This should be an indication of the level of attenuation expected from the high pass filtered *WMAP* map cross-correlated with the NVSS map. The high pass filtered NVSS map was also cross-correlated with the HEAO map in order to estimate the attenuation expected from the high pass filtered *WMAP* map cross-correlated with the HEAO map. This attenuation was $\sim 2\%$, again negligible. Because the resolution of the K and Ka bands (0.88 and 0.66 degrees) are not negligible compared to the pixel size (1.3 degrees), the former test might not be appropriate for the filtered *WMAP*/NVSS CCF. However, when a filtered X-ray map (which has a FWHM angular resolution of 3 degrees) was correlated with the NVSS map, the CCF(0) is attenuated by only 1.5% with respect to the unfiltered CCF(0), again a neglible amount. So, we conclude that the

high pass filtering has a negligible effect on the above results.

5.3. Comparison with Other Measurements and Predictions

There is evidence of excess small-angular-scale fluctuations in the three-year *WMAP* Q-band data (Huffenberger et al. 2006; Hinshaw et al. 2007). Under their assumption of uncorrelated (i.e., Poisson only) fluctuations, it is straightforward to translate this excess to equivalent Q-band Rayleigh-Jeans temperature fluctuations in a one square degree beam. The Hinshaw et al. (2007) estimate implies rms fluctuations of $T_{RJ} \sim 4.5$ μK while the Huffenberger et al. (2006) estimate corresponds to $T_{RJ} \sim 4.0$ μK. That these two estimates are consistent with our rough estimate above should be tempered by the assumptions required to arrive at the latter. To truly unravel the excess small-scale fluctuations, a sensitive, blind radio survey at the high frequencies normally used in CMB studies would be very helpful. In the meantime, our results suggest no unpleasant surprises in the *WMAP* frequency range.

CMB measurements at smaller angular scales are more prone to contamination by foreground sources because the power spectrum, $\ell(\ell+1)C_\ell$, of unclustered sources is proportional to ℓ^2. There is a substantial literature on the effect of radio sources on the microwave power spectra reported by the CBI, DASI, and ACBAR groups, for instance. This is nicely summarized by Toffolatti et al. (2005). Toffolatti and his colleagues also attempt to model the expected contributions to high ℓ fluctuations from various classes of foreground sources. These predictions cannot be directly compared to our measurement because the models, like the microwave measurements, exclude radio sources down to a limit well below the ~1 Jy cutoff we employed. For instance, the CBI group (Readhead et al. 2004; Mason et al, 2003) removed all sources down to ~30 mJy (and many weaker sources as well) from their images before calculating the power spectrum. Therefore the measured (Readhead et al. 2004) and predicted (Toffolatti et al. 2005) levels of fluctuation lie roughly a factor 10 lower than our value projected to $\ell = 1000$ and a frequency of 30 GHz.

On the other hand, we can compare our value of $\sim 5(\nu/40.7$ GH$z)^{-2.1}$ μK to values of rms fluctuation predicted by Toffolatti et al. (1998), since these predictions exclude only sources above 1 Jy. Figure 6 of that paper shows that predicted level of fluctuations on a ~1° scale is ~4.5 μK. When we scale from 44 GHz to 40.7 GHz using a $\beta = -2.1$ temperature spectrum, and correct from the Gaussian angular scale Toffolatti used to a 1° top hat beam, we obtain ~5.3 μK, which is consistent with our lower limits and similar to our rough estimate of total fluctuations. Further, if we compare temperature fluctuations shown in his Figures 5 and 6 for 30, 44, 70 and 100 GHz, we find that the implied spectral index on scales of ~1° is $\beta \sim -1.9$, close to our best-fit value, and inconsistent with a normal synchrotron spectrum. We conclude that we have

found no evidence in the *WMAP* frequency range of a large radio source contribution to the microwave sky not captured in Toffolatti's 1998 models. The COSMOSOMAS team (Hildebrandt et al., 2007) also find radio source contributions consistent with De Zotti et al. (2005), an updated version of Toffolatti's work, in the COSMOSOMAS frequency range of 11–16 GHz. At these low frequencies, it would not be surprising to find that the average spectral index of foreground radio sources more closely resembles a synchrotron spectrum with $\beta = -2.7$ or -2.8. Instead, the data in their Figure 15 seem to suggest an even flatter spectral index, with $\beta \sim -1.4$.

In the decade since 1998, refined models of source counts at high microwave frequencies have been published by, among others, Cleary et al. (2005), De Zotti et al. (2005), and Waldram et al. (2007), and while this paper was under review, Sadler et al. (2007). Waldram's source counts are extrapolated from 15 GHz observations and may contain a selection bias against sources brighter than 0.1 Jy, those most likely to dominate the foreground. Sadler's recent and important results show that 95 GHz source counts at fluxes above 0.08 Jy—the range of interest for us—are lower than found in previous studies, including that of De Zotti et al. (2005). We note, however, that Sadler's was not a blind survey at 95 GHz, but relied on sources selected at 20 GHz. Sadler et al. also estimated the residual temperature fluctuations due to 95 GHz sources under the assumption of Poisson statistics. Expressed as Rayleigh-Jeans temperature fluctuations in 1 deg², their estimate is 0.62 μK and is clearly consistent with the lower limit in Figure 8. If the power spectrum is $\beta = -2.1$, this corresponds to 40.7 GHz fluctuations of 3.7 μK, slighly below but consistent with the estimates of Hinshaw et al. (2007) and Huffenberger et al. (2006), as well as with the rough estimate of this paper. Cleary et al. (2005) estimate the temperature fluctuations at 33 GHz, when expressed in equivalent Poisson fluctuations in 1 deg², to be 1.4 μK. While slightly below our lower limit in Figure 8, their estimate is for a flux cutoff of 20 mJy and so is not inconsistent with this limit. De Zotti et al. (2005) and Waldram et al. (2007) do not provide calculations of the expected fluctuation level in the microwave sky; however, we can compare their source counts with those of Toffolatti et al. (1998) at the appropriate frequency and in the relevant range of flux density. In general, the more recent source counts fall roughly a factor 1.5–2.0 below Toffolatti's. Thus the expected level of fluctuations would be 20%–40% lower than Toffolatti's 1998 value, but still in agreement with our results. Obviously, the roughness of our estimate does not allow us to discriminate between these various models. What we can say is that, up to 90 GHz at least, there are no surprises in the form of unexpected populations of high frequency sources and that the source count estimates deduced from lower frequency radio catalogs are reliable.

REFERENCES

Allen, J., Jahoda, K., & Whitlock, L. 1994, Legacy, 5, 27
Boldt, E. 1987, Phys. Rep., 146, 215
Boughn, S. 1999, ApJ, 526, 14
Boughn, S., & Crittenden, R. 2002, Phys. Rev. Lett., 88, 021302
Boughn, S., & Crittenden, R. 2004a, ApJ, 612, 647
Boughn, S., & Crittenden, R. 2004b, Nature, 427, 45
Boughn, S., Crittenden, R., & Koehrsen, G. 2002, ApJ, 580, 672
Cleary, K., et al. 2005, MNRAS, 360, 340
Condon, J. 1984, ApJ, 287, 461
Condon, J., et al. 1998, AJ, 115, 1693
De Zotti, G., et al. 2005, A&A, 431, 893
Dunlop, J., & Peacock, J. 1990, MNRAS, 247, 19
Finkbeiner, D. 2003, ApJS, 146, 407
Jahoda, K., & Mushotzky, R. 1989, ApJ, 346, 638
Hildebrandt, S., et al. 2007, submitted to MNRAS (astro-ph/07061873)
Hinshaw, G., et al. 2007, ApJS, 170, 288
Huffenberger, K., Eriksen, H., & Hansen, F. 2006, ApJ, 651, L81

Lopez-Caniego, M., et al. 2007, ApJS, 170, 108
Mason, B., et al. 2003, ApJS, 591, 540
Massardi, M., et al. 2007, MNRAS in press (astro-ph/07093485)
Peebles, P. J. E. The Large-Scale Structure of the Universe, (Princeton, NJ: Princeton Univ. Press, 1980)
Piccinotti, G., et al. 1982, ApJ, 253, 485
Readhead, A., et al. 2004, ApJ, 609, 498
Sadler, E., et al. 2007, submitted to MNRAS (astro-ph/07093563)
Toffolatti, L., et al. 1998, MNRAS, 297, 117
Toffolatti, L., et al. 2005, A&A, 438, 475
Trushkin, S. 2003, Bull. Spec. Astrophys. Obs.—North Caucasus, 55, 90 (astro-ph/0307205)
Voges, W., et al. 1996, IAU Circ., 6420, 2
Waldram, E., et al. 2007, MNRAS, 379, 1442
White, R., & Stemwedel, S. 1992, in ASP Conf. Ser. 25, Astronomical Data Analysis Software and Systems I, ed. D. Worral, C. Biemesderfer, & J. Barnes (San Francisco: ASP), 379